Supplementary Information:

A Class of High Performance Metal-Free Oxygen Reduction Electrocatalysts based on Cheap Carbon Blacks

Xiujuan Sun[1,2,3], Ping Song[1,2], Yuwei Zhang[1,2], Changpeng Liu[1,2], Weilin Xu[1,2]*, Wei Xing[1,2]*

[1] State Key Laboratory of Electroanalytical Chemistry, Changchun Institute of Applied Chemistry, Chinese Academy of Science, 5625 Renmin Street, Changchun 130022, P.R. China.

[2] Jilin Province Key Laboratory of Low Carbon Chemical Power, Changchun Institute of Applied Chemistry, Chinese Academy of Science, 5625 Renmin Street, Changchun 130022, P.R. China.

[3] Graduate University of Chinese Academy of Science, Beijing, 100049, China.

*To whom correspondence should be addressed. E-mail: weilinxu@ciac.jl.cn (W. X.); xingwei@ciac.jl.cn (W. X.)

1. Experimental

1.1. Materials

The carbon black BP2000 was purchased from Asian-Pacific Specialty Chemicals Kuala Lumpur, Acetylene carbon black (50% compressed) was purchased from Strem Chemicals. Ammonium fluoride (NH_4F) was purchased from Beijing Chemical Works, China, melamine ($C_3H_6N_6$), was purchased from Sinopharm Chemical Reagent Co. LTD, Postassium hydroxide (KOH) was purchased from Beijing Chemical Works, and Nafion solution (5 wt %) were obtained from Sigma-Aldrich. All the chemicals were used as delivered without further treatment. Ultrapure water with the specific resistance of 18.23 MΩ·cm was obtained by reversed osmosis followed by ion-exchange and filtration. Rotating disk electrode of glassy carbon (RDE, 4 mm in diameter) was purchased from Tianjin Aida Hengsheng Tech. Co., China.

1.2. **Preparation of metal-free nitrogen, fluorine-doped carbon materials**

The synthesis of CB-NF was based on a two-step procedure with CB, melamine ($C_3H_6N_6$) and ammonium fluoride (NH_4F) as initial materials. Firstly, N-doped carbon blacks were obtained as follows: a given amount of carbon blacks and appropriate melamine were ground together in an agate ball mill for about 2 h. After that the pyrolysis of the obtained mixture was performed at 900 ℃ for 1 h under argon atmosphere with flow rate of 80 mL/min. Secondly, the as-obtained CB-N was added into the NH_4F solution while keeping fierce stirring overnight. The final mixture was dried under vacuum at 40 ℃ and then pyrolysized at 400 ℃ for 30min, 900 ℃ for 1h under argon atmosphere with flow rate of 80 mL/min. For comparison, CB, CB-N or CB-F was also obtained in a similar way with or without melamine or ammonium fluoride.

1.3. **Characterization of the nitrogen, fluorine-doped carbon materials**

XRD measurements were performed on a Rigaku-Dmax 2500 diffractometer with Cu Kα radiation (λ = 0.15405 nm) from 10 to 90 degree at a scanning rate of 5 degree per minute. X-ray photoelectron spectroscopic (XPS) measurements were performed on a AXIS Ultra DLD (Kratos company) using a monochromic Al X-ray source. The morphology and dimensions of as-prepared samples were obtained using a field emission scanning electron microscopy

instrument (SEM, XL30) with energy-dispersive X-ray analyzing (EDX) system, operating at an accelerating voltage of 10 kV. The Brunauer-Emmett-Teller (BET) surface areas and pore volumes were obtained from 77 K N_2 sorption isotherms using ASAP 2020 instrument.

1.4. **Electrochemical measurements**

The activity for the oxygen reduction reaction (ORR) was evaluated by voltamperometry by the high-surface-area nitrogen fluorine-doped carbon materials as electrodes. Fabrication of the working electrodes was done by pasting catalyst inks on a glassy carbon rotating disk electrode (4 mm in diameter). Its apparent surface area (0.1256 cm^2) was sued to normalize the ORR activity of the catalysts. The carbon ink was formed by mixing 5 mg of nitrogen fluorine-doped carbon materials catalysts, 100 μL of a 5 wt % Nafion solution in alcohol, and 900 μL of ethanol in a plastic vial under ultra-sonication. A 10-μL aliquot of the carbon ink was dropped on the surface of the glassy carbon rotating disk electrode, yielding an approximate catalyst loading of 0.05 mg. For comparison, a commercially available platinum/carbon catalyst, nominally 20 wt % on carbon black from E-TEK was used. The platinum based ink was obtained by mixing 1 mg catalyst, 100 μL of a 5 wt % Nafion solution in alcohol, 900μL of ethanol. Then, a 15-μL aliquot of the platinum ink was dropped on the glassy carbon rotating disk electrode, yielding an approximate loading of 0.015 mg or 24 ug Pt cm^{-2}. The electrolyte was 0.1 M KOH solution; the counter and the reference electrodes were a platinum wire and a SCE electrode, respectively. The potential of the electrode was controlled by an EG&G (model 273) potentiostat/galvanostat system. Cyclic voltammetry was performed from 0.2 to -1.0 V at 50 mV s^{-1} after purging the electrolyte with O_2 or N_2 gas for 30 min. Voltamperometry measurements were performed by using the rotating disk electrode (RDE) at different rotating speeds from 225 to 2500 rpm in an O_2-saturated electrolyte from 0.2 to -1.0 V (vs SCE) at a sweep rate of 5 mV/s.

1.5. Membrane assembly electrode (MEA) preparation and fuel cell tests

In this work, poly (arylene ether ketone) (PAEK) containing pendant quaternary ammonium groups was used to prepare anion-exchange membrane with thickness of about 30 um for alkaline direct methanol fuel cells tested here(Ref. S5). Before fabrication of MEA, the membrane was soaked in 2 M KOH for at least one week to change it to OH^-. The membrane was then rinsed and stored in Millipore water two days before later use. Its hydroxide ion conductivity is above 10^{-2}S/cm at room temperature. Carbon supported Pt (20 or 60 wt % on Vulcan XR72, E-TEK, USA) or BP2000-NF was used to prepare the catalyst ink. Inks were made by mixing the catalysts powder, ethanol and 5% Nafion (Aldrich, USA) suspension. The catalyst layer was prepared on non-wet-proofed Toray 90 carbon paper (E-TEK, USA). After the desired amount of catalyst loading was achieved, the anode, cathode and membrane were sandwiched together and pressed at 130 kg/cm^2 for 5 min at room temperature.

A stainless steel cell consisting of two compartments with 2 mm parallel channel flow field for methanol and oxygen flow was employed in this work. The active cross-section area of the cell was 6.25 cm^2. The fuel used was 2 M methanol in 2 M KOH at an operation temperature of 60^{o}C, unless otherwise specified. A peristaltic pump (Watson Marlow, UK) was used to supply methanol to anode. The pure dry oxygen was supplied to the cathode with a flow rate of 100 mL/min. An in-house-made water bath and temperature controller was used to maintain the temperature at 60^{o}C. The open circuit voltages (OCV) were recorded after stable values were reached. All the cell polarization data and stability data were obtained after 24h of cell conditioning.

2. **X-ray photoelectron spectroscopy (XPS) characterization of catalysts**. The survey scans spectra from XPS for BP2000-NF (Fig. S1a) reveal the presence of C 1s, O 1s, N 1s and F 1s without any other impurities on the BP2000-based catalysts. It was further revealed from XPS that the oxygen, nitrogen and fluorine contents in BP2000-NF are about 4.4 at%, 4.3 at% and 0.2 at%, respectively (Fig. S1b).

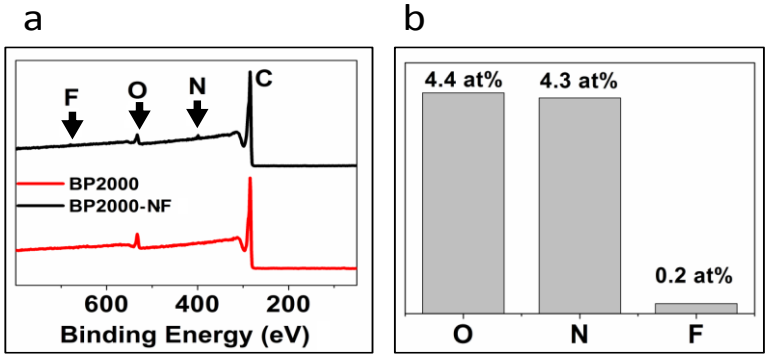

Fig. S1. (**a**)The survey scans spectra from XPS for BP2000 and BP2000-NF. (**b**) Chart showing the percentages of O, N and F in the BP2000-NF obtained from XPS.

3. Structural characterization of BP2000-NF.

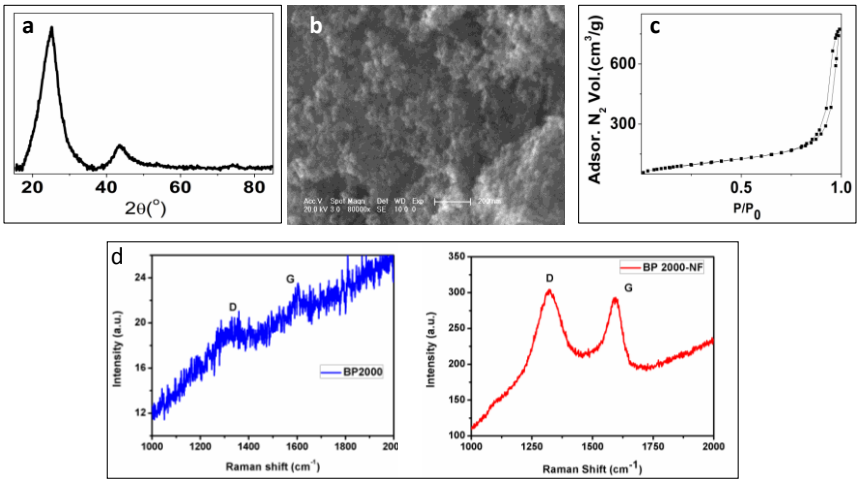

Fig. S2. Structural characterization of BP2000-NF. (a) XRD spectrum of BP2000-NF. (b) Typical SEM image of BP2000-NF. (c) Nitrogen sorption isotherm. (d) Raman spectrum for BP2000 (blue) and BP2000-NF(red).

It has been well known that G band from Raman spectrum represents the graphitic carbon in the material (***Angew. Chem. Int. Ed.*** 2012, 51, 1-6). Above figure clearly shows the intensity of G band for BP2000-NF increased lot compared with the original BP2000, which unambiguously indicates that there exists high content of graphitic carbon in BP2000-NF.

4. Voltamperograms for oxygen reduction on BP2000, BP-N and BP-F in O_2-saturated 0.1 M KOH at various rotation speeds.

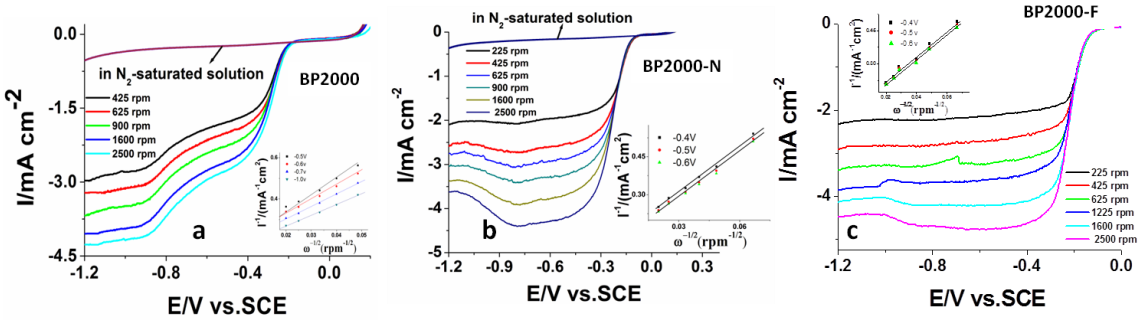

Fig. S3. Voltamperograms for oxygen reduction on BP2000 (a), BP-N (b) and BP-F(c) in O_2-saturated 0.1 M KOH at various rotation speeds with scan rate of 5 mV/s. For BP2000 and BP2000-N, LSVs at different electrode rotation rates in N_2-saturated solution were also presented and indicated by arrow. Insets: K-L plots at different potentials.

From Fig. S3, we can see the ORR on pure BP2000 is a two-step two-electron process (the number of transferred electrons is about 2.6 at 0.5 V, 3.7 at 0.6 and 0.7 V from the K-L plots.), while on BP-N and BP-F it is a four-electron process with number of transferred electrons 3.9 and 4.0 respectively. The glitches on curves in Fig. S3c are due to the occasional machine noise, which do not affect the reading of diffusion-limited plateau currents.

5. The comparison of BP2000-NF with the best non-Pt ORR catalysts reported before.

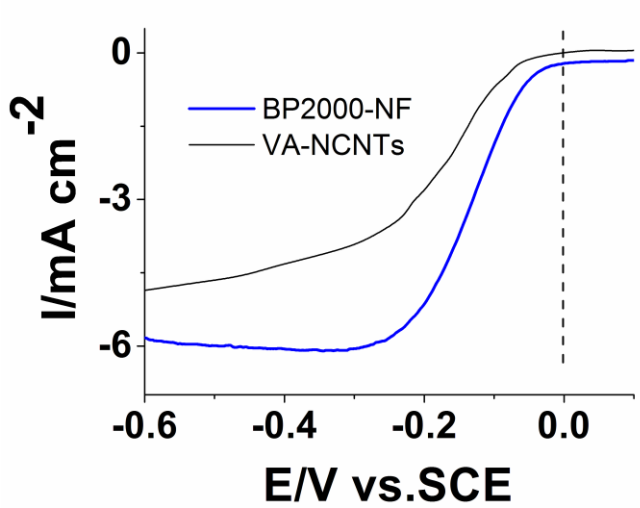

Fig. S4. A comparison of polarization curves between BP2000-NF in O_2-saturated 0.1 M KOH and Vertically-aligned nitrogen-doped carbon nanotubes (VA-NCNTs) from Ref. S1 (*Science* **323**, 760 (2009), in air-saturated 0.1 M KOH) with electrode rotation speed of 1600 rpm. Scan rate for BP2000 is 5 mV/s, for VA-NCNTs is 10 mV/s. The data from Ref. S1 were obtained with software "xyExtract" by Wilton P. Silva and then the potential values were converted to versus SCE according to standard reference electrode potentials.

As shown in Fig.S4, the performance of BP2000-NF for ORR is on the same level as that of VA-NCNTs. The BP2000-NF is more than 10,000 times cheaper or abundant than VA-NCNTs. These facts indicate the BP2000-NF is a much better alternative to Pt for ORR than VA-NCNTs.

6. Analysis of peroxide using Rotating ring disk electrode (RRDE).

Rotating ring disk electrode (RRDE) tests were conducted on RRDE-3A apparatus (ALS Company, Japan) with the Glassy Carbon disk and Pt ring electrode (the diameter is 4 mm for disk). Voltamperometry measurements were performed from 0.2 to -1.2 V at 50 mV s^{-1} after purging the electrolyte with O_2 or N_2 gas for 30 min by using the rotating ring-disk electrode (RRDE) at scan rate of 1600 rpm and a sweep rate of 5 mV/s.

For the calculation of yields of H_2O_2 on different catalysts, based on both ring and disk currents from RRDE, the percentage of HO_2^- generated from ORR was estimated by the following equations:

$$HO_2^-\% = 200 \times \frac{i_R / N}{i_D + i_R / N}$$

Where i_D is the disk current density, is the ring current density and N is the current collection efficiency of the Pt ring disk. N was 0.37 from the reduction of $K_3Fe\,[CN]_6$.
All the current densities have already been normalized to the electrode surface area.

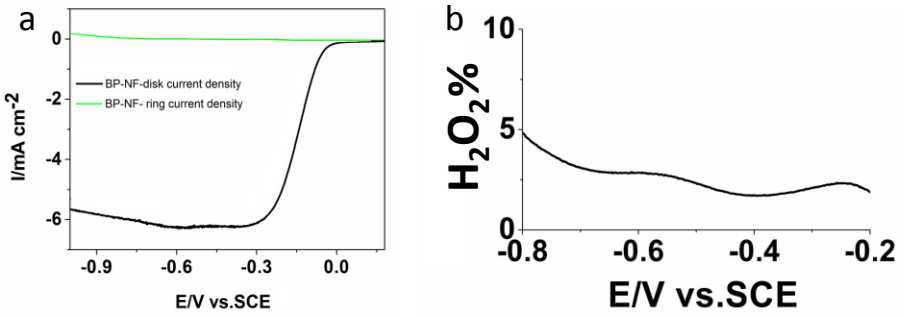

Fig. S5. Analysis of hydrogen peroxide with RRDE for BP2000-NF with rotation speed of 1600 rpm in 0.1M KOH saturated with oxygen.

As shown in Fig. S5, the yield of H_2O_2 on BP2000-NF is very low.

7. **The effect of treating temperature on the F doping.** At low treating temperature for F-doping, it was found the doped F is mainly in the semi-ionic and covalent C-F state (black curve Fig. S6). So the anion $F^{\delta-}$ ($\delta<1$) or ionic C-F bond was probably formed at high temperature due to the partial break of covalent C-F bond formed at low treating temperature. In the ionic C-F bond the $F^{\delta-}$ still bonds with $C^{\delta+}$ tightly but with more ionic content compared with covalent ones. Obviously the $F^{\delta-}$ in the ionic or semi-ionic C-F bond is different from the free F^- adsorbed on carbon physically from solution. That is why it is very stable even in aqueous basic solution.

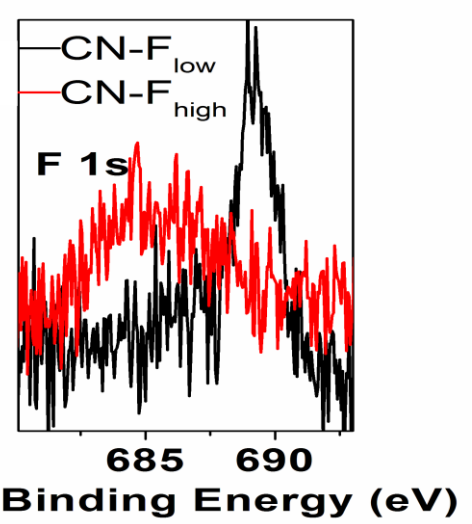

Fig. S6. XPS spectra of BP2000-NF obtained different treating temperatures for F-doping. Black curve is for the one treated at low temperature (400°C). The doped-F is mainly semi-ionic C-F bond. At high temperature (900°C) the obtained F is mainly in ionic state (Red).

8. A comparison of ADMFC performance with Pt black cathode.

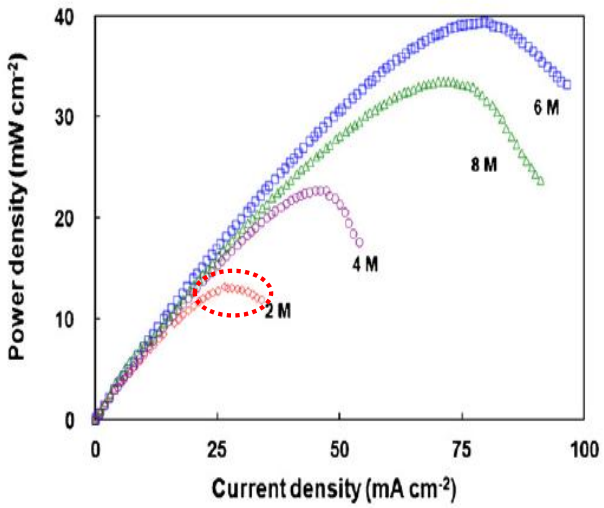

Fig. S7. Effect of KOH concentration on (d) power density at 60°C (anode: 2 M methanol in KOH at a flow rate of 5 mL min^{-1}, cathode: humidified oxygen with a flow rate of 100 mL min^{-1}, electrolyte: PVA/0.05CNT/KOH). Cited from Ref. S7 (*J. Power Sources* **202**, 1 (2012)).

In all these ADMFCs, the anode catalyst is PtRu (1:1) black, 5 mg/cm^2, the cathode is Pt black, 5 mg/cm^2. As shown in this figure, the performance of the cell with 2 M KOH is even worse than that based on BP2000-NF cathode shown in Fig. 4.

9. The ORR of Acetylene carbon (AC) black-based metal-free catalysts in alkaline medium: (AC-NF)

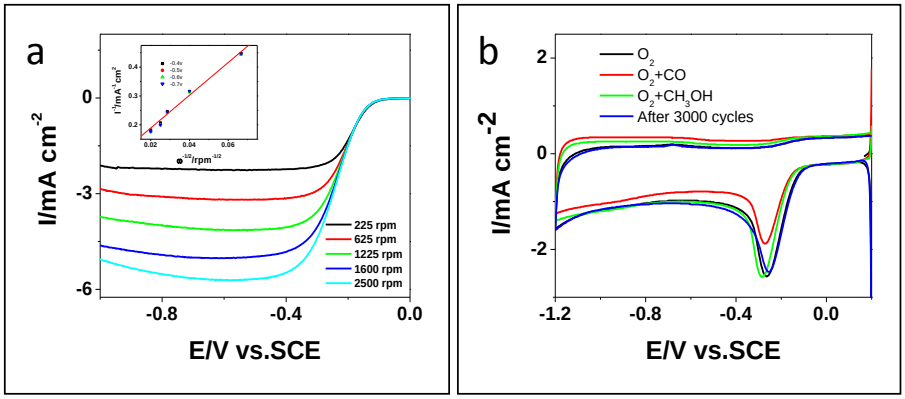

Fig. S8. (a) Voltamperograms for oxygen reduction on AC-NF in O_2-saturated 0.1 M KOH at various rotation speeds with scan rate of 5 mV/s. Inset: K-L plots at different potentials. (b) The tolerance and stability of AC-NF in O_2-saturated (black), or CO- and O_2-saturated (red), 3 M methanol O_2-saturated (green) or after 3000 cycles of CV 0.1 M KOH with scan rate of 50 mV/s.

Figure S8 shows that the AC-NF also shows high activity and stability of ORR in alkaline condition, which is very close to that on BP2000-NF.

10. Quantum Mechanics Calculations

The electrocatalytic activity of CB-NF has been carried out by density functional theory (DFT) method with Gaussian 09 *(S6)*. The XPS shows three types of O in the form of C-OH, COOH and C=O, and the ratio of O:N is nearly equal to 1. One pure CB model (65 atoms) with a vacancy effect has been constructed (denoted as compound **a** (CB) in Fig. S9), and N-doped CB shows an almost equal ratio for doped nitrogen atoms and edge oxygen atoms (denoted as compound **b** (CB-N)). In addition, F is supposed to suspend over the surface of CB to form F- and NF-co-doped CB (denoted as compounds **c** (CB-F) and **d** (CB-NF)). Based on the previous results (*S7*), the preferred chemisorption mode of O_2 on CB is a side-on adsorption (Yeager model), and the three corresponding O_2-adsorbed systems are denoted as **a+O_2** (based on pure CB), **b+O_2** (based on CB-N), **c+O_2** (based on CB-F) and **d+O_2** (based on CB-NF) shown in Fig. 2C. The larger sizes such as **a+O_2-1** (107 atoms) in Fig. S9 have also been tested, which reveal the same trend comparing with smaller size models (Fig. S10). We mainly focus on the interaction in the active sites, and more peripheral carbon atoms will play less prominent role in the active site. In the current work, the smaller ones have been chosen to investigate the activity of ORR, which should be large enough to include the active sites (*S8-S12)*. A conductor-like screening model (COSMO) is performed to consider the influence of the aqueous solution. The solvation effect stabilizes all the systems, and it shows the similar trend with the gas phase (Fig. S10). Herein, the discussion is based on small-sized models with water as solvent and all the data are shown in Table 1.

From Table 1, before O_2 adsorbed over the CB models, the energy gap (E_g) of compound **d** (0.770 eV) is smaller than that of compounds **c** (1.556 eV) and **b** (1.584 eV) and compound **a** (1.726 eV), which predicts higher electrocatalytic activity of CB as a result of synergetic effect between doped N and F atoms (*S13*). O_2 in compound **a+O_2** keeps the bond length of 1.217 Å as nearly an isolated molecule. The charge rearrangement for N- and F-doping lengthens the bond length O_2 to 1.241 Å and 1.254 Å, respectively, and the NF-co-doping in compound **d+O_2** lengthens O_2 to 1.258 Å. In other words, doped atoms induces the activation on O_2 for CB, and

the CB-NF performs better electrocatalytic activity for ORR comparing with CB-F, especially CB-N. The more electronegativity for N and F atoms induces the neighboring C atoms with positive charges, indicating better charge-transfer properties *(S12)*, and O_2 molecule prefers to attract at the positive C sites (*S8, S13, S14*). Furthermore, for the synergetic effect between N and F, the interactions between the CB models and O_2 have been investigated by Natural Bond Orbitals (NBO), and the main orbital interactions between the two segments have been listed in Fig. S11. It can be observed that there is nearly no interaction between CB and O_2 in **a+O_2** (Fig. S11), and N- and F-doping evokes 3-center-bond of C_1-C_2-C_3 interacts with σ*-bond of O_2 (**b+O_2** and **c+O_2** in Fig. S11). Interestingly, the NF-co-doping in compound **c+O_2** (Fig. S11) products the interaction between the F and N, i.e. the lone electron pair of F and σ^*-bond of adjacent C-N bonds. Moreover, the synergetic effect between N and F enhances the attraction interaction between O_2 and adjacent C and N, in other words, it can promote O_2 to adsorb on the surface of CB-NF. The negative charge (-0.33 e) for O_2 in compound **d+O_2** is resulted from the stronger effect for N, F and C in O_2 comparing with those in compounds **b+O_2** (-0.21 e) and **c+O_2** (-0.31 e), indicating better electron transfer from CB-NF to O_2. The 0.02 e the CB segment in compound **a+O_2** affords to O_2 further confirms the weak physisorption between them, nearly without any charge transfer. Heteroatom (N and F) doping induces larger adsorption energy for O_2 than pure CB, and NF-co-doping enhances larger adsorption energy (-0.39 eV), indicating stronger effect in O_2. Moreover, the NBO analysis displays a charge of -0.61 e for F in CB-NF, and the interaction between F and adjacent C-N bond leads F still bonding tightly with adjacent C (Fig. S11). That means the C-F bond formed is not a pure covalent one and shows some ionic character, consistent with the results from XPS. Obviously the doped F in the ionic C-F bond is different from the physisorbed free F^- from solution.

To sum up, all of these theoretical results preliminarily confirm the electrocatalytic activity order of CB-NF>CB-F≥CB-N>CB, consistent with the experimental observations of exceptionally high electrocatalytic activity of BP2000-NF for ORR.

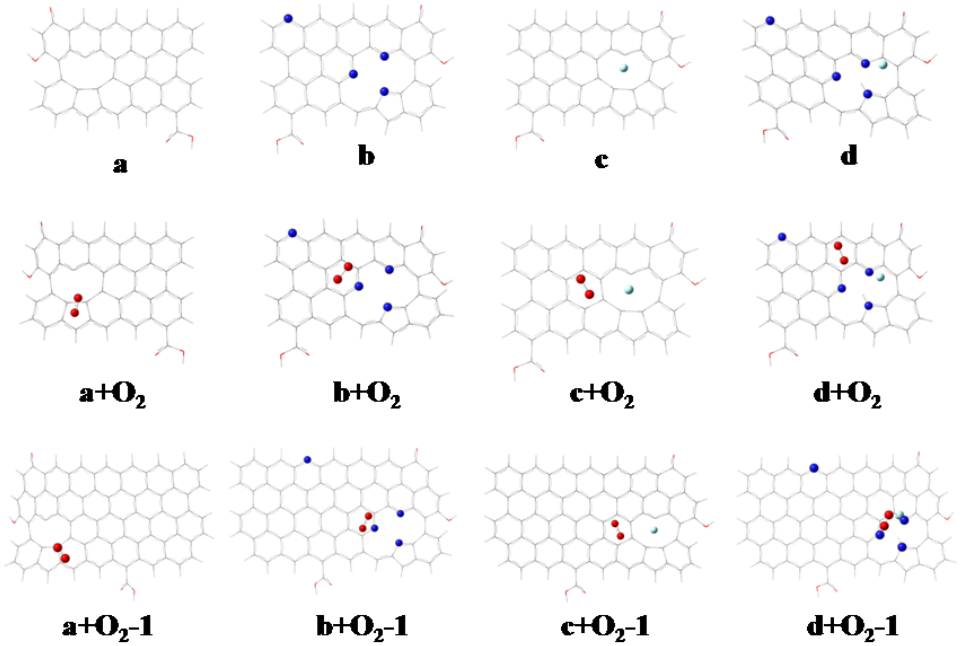

Fig. S9. The optimized geometries for four CB models **a**, **b**, **c**, **d** and corresponding O_2 adsorption structures (**a+O$_2$**, **b+O$_2$**, **c+O$_2$** and **d+O$_2$**) with larger sizes.

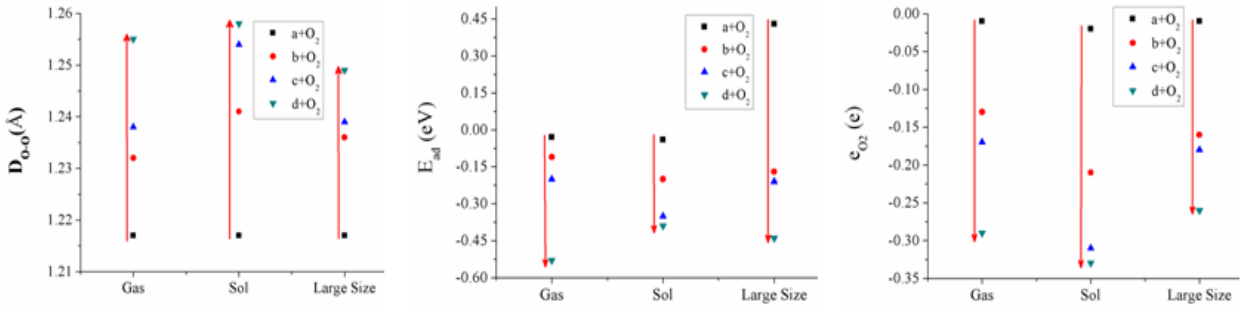

Fig. S10. The tendency of geometry parameters for **a+O$_2$**, **b+O$_2$**, **c+O$_2$** and **d+O$_2$** in gas and solution phase as well as the larger size models. D_{O-O}: The bond distance for O_2. e_{O2}: The charge O_2 possesses. E_{ad}: The adsorption energy, and it is equal to E_{ad}= E(CB-O_2)-E(CB)-E(O_2), in which E(CB-O_2), E(CB) and E(O_2) is the total energy for CB-O_2 system, separated CB and separated O_2 molecule.

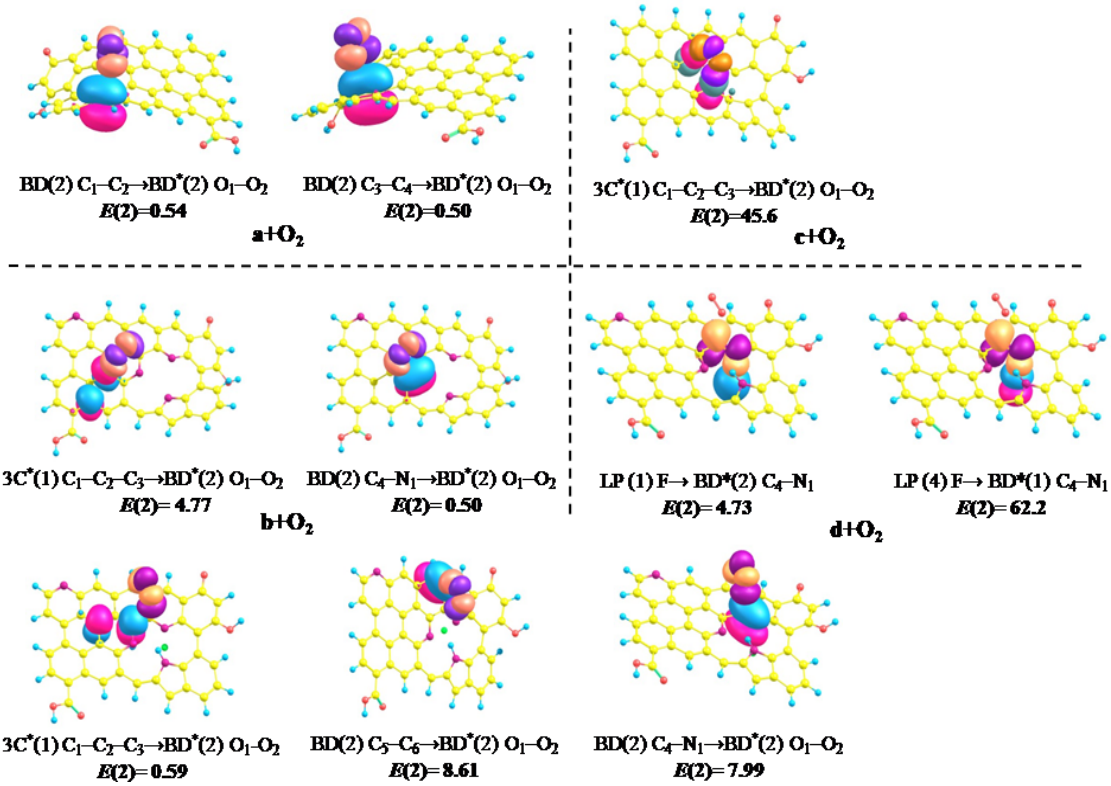

Fig. S11: The main Natural Bond Orbital (NBO) for the interaction between O_2 and CB systems. Yellow, red, violet, green and blue colors denote C, O, N, F and H atoms. (3C*: The 3-center antibond; BD: 2-center bond; BD*: 2-center antibond; LP: 1-center valence lone pair; *E*(2): The second-order perturbation energy (kJ ·mol^{-1}), $E(2)=E_{ij}=q_iF_{ij}^2/(\varepsilon_j-\varepsilon_i)$)

11. The Pt-loading issue.

In this work we used a Pt-loading of 24ug/cm^2 as a standard reference (Ref. S15) since we have observed a saturation phenomenon as shown in the following Fig. S12.

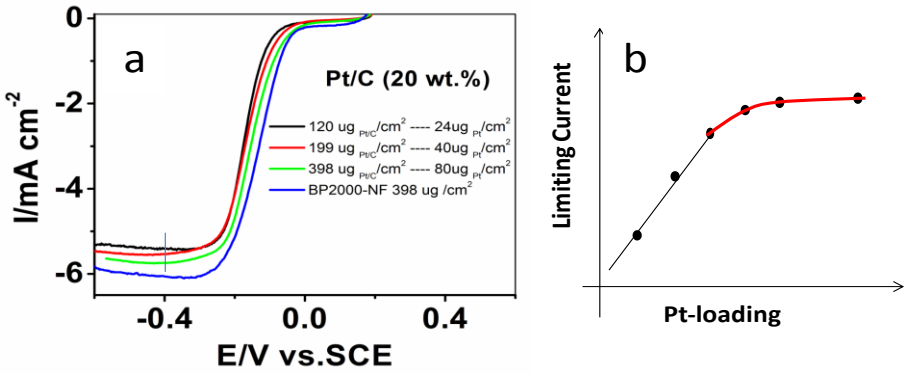

Fig. S12. (a) The comparison of Pt/C at different loadings with BP2000-NF. (b) The dependence of limiting currents on the Pt-loadings on electrode. The red curve shows a saturation plateau at high loading.

12. The performance of BP2000-NF in acid condition.

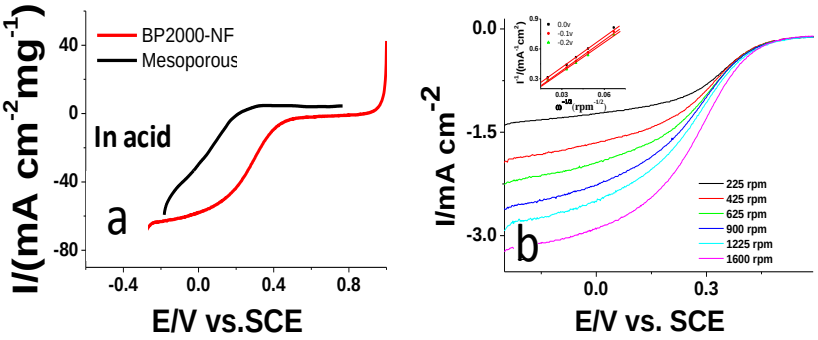

Fig. S13(a) A polarization comparison of BP 2000-NF (red curve) with metal-free Meso-EmG (*J. Am. Chem. Soc.* **133**, 206 (2011)) obtained from very expensive ionic liquid (black) with electrode rotation speed of 1600 rpm. Scan rates: 5 mV/s. Red curve is in O_2-saturated 0.5 M H_2SO_4, black curve in 0.1 M $HClO_4$. (b) Voltamperograms for oxygen reduction on BP2000-NF in O_2-saturated 0.5 M H_2SO_4 at various rotation speeds with scan rate of 5 mV/s. Inset: K-L plots at different potentials.

For BP 2000-NF in acid condition, we can see from Fig. S13 it is a highly active and selective non-Pt or metal-free catalyst for the electrochemical synthesis of hydrogen peroxide with a two-electron process. Compared with one of the best metal-free ORR catalyst for ORR to produce hydrogen peroxide (*J. Am. Chem. Soc.* **133**, 206 (2011)), the BP2000-NF possesses much higher onset potential and steady-state diffusion current (Fig. S5A), indicating a much higher intrinsic activity of BP 2000-NF for the ORR reduction to produce hydrogen peroxide in acid condition.

13. To rule out the contamination of Pt from counter electrode. Pt has been extensively used as counter electrode for ORR study (Ref.S15). In order to rule out the contamination of Pt from counter

electrode, we compared the performance of the BP2000-NF with Au and Pt as counter electrode, respectively.

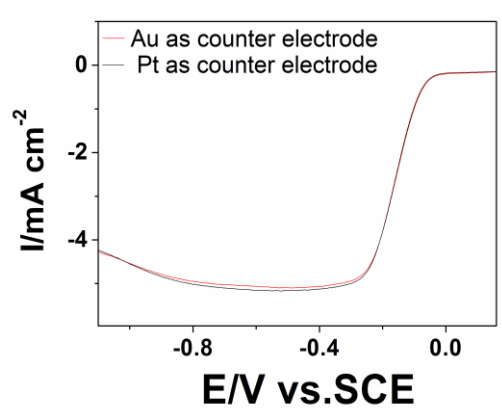

Fig. S14. The comparison between Au and Pt Counter electrode. This figure shows there is no effect of the counter electrode on the performance of catalyst. This experiment is done by testing with Au foil counter electrode first, then with Pt foil counter electrode in 0.1 M KOH for BP2000-NF on glassy carbon electrode.

From it one can see clearly the high performance of our catalyst is not due to the contamination of Pt from counter electrode.

14. The effect of N or F content on the performance of catalysts.

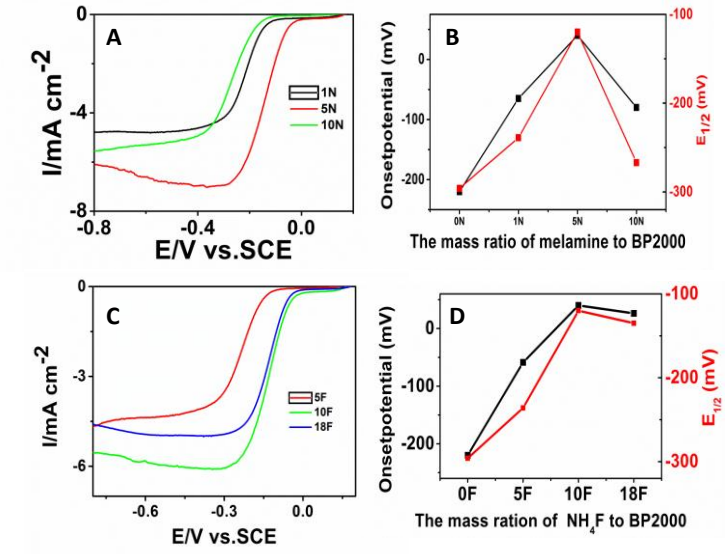

Fig. S15 Variation of N or F content. The effect of N or F content on the performance of BP2000-based catalysts. It can be seen the performance (the onset potential and half-wave potential) of catalyst will decrease when the N or F content is too high or too low.

References:

S1. K. Gong, F. Du, Z. Xia, M. Durstock, L. Dai, *Science*, **323**, 760 (2009).
S2. Y. Li *et al.*, *Nature Nanotechnology*, **7**, 394 (2012).
S3. W. Yang, T. P. Fellinger, M. Antonietti, *J. Am. Chem. Soc.* **133**, 206 (2011).
S4. T. Fellinger, F. Hasche, P. Strasser, M. Antonietti, *J. Am. Chem. Soc.* **134**, 4072 (2012).
S5. J. Wang, J. Wang, S. Zhang, *J. Membrane Science*, **415-416**, 205 (2012).
S6. M. J. Fisch et al., Revision C.01; Gaussian, Inc., Wallingford, CT, 2010
S7. S. J. Lue, W. Pan, C. M. Chang, Y. L. Liu, *J. Power Sources* **202**, 1 (2012).
S8. L. R. Radovic, B. Bockrath. *J. Am. Chem. Soc*. **127**, 5917 (2005).
S9. M. A. Ribas, A. K. Singh, P. B. Sorokin, B. I. Yakobson. *Nano Res*. **4**, 143 (2011).
S10. A. Cavallin, M. Pozzo, C. Africh, A. Baraldi, E. Vesselli, C. Dri, G. Comelli, R. Larciprete, P. Lacovig, S. Lizzit, D. Alfè, *ACS Nano* **6**, 3034 (2012).
S11. L. Wang, K. Lee, Y.-Y. Sun, M. Lucking, Z. Chen, J. J. Zhao, S. B. Zhang. *ACS Nano* **3**, 2995 (2009).
S12. V. V. Strelko, V. S. Kuts, P. A. Thrower. *Carbon*, **38**, 1499 (2000).
S13. S. Yang, X. Feng, X. Wang, K. Müllen, *Angew. Chem., Int. Ed.* **50**, 5339 (2011).
S14. S. Wang et al., *Angew. Chem., Int. Ed*. **51**, 1 (2012).
S15. G. Wu, K. L. More, C. M. Johnston, & P. Zelenay, *Science* **332**, 443 (2011).